ACS APPLIED MATERIALS & INTERFACES

Research Article

www.acsami.org

Enhanced Thermal Stability under DC Electrical Conductivity Retention and Visible Light Activity of Ag/TiO_2@Polyaniline Nanocomposite Film

Mohd Omaish Ansari,[†] Mohammad Mansoob Khan,[†] Sajid Ali Ansari,[†] Kati Raju,[‡] Jintae Lee,[†] and Moo Hwan Cho[†,*]

[†]School of Chemical Engineering and [‡]School of Materials Science and Engineering, Yeungnam University, Gyeongsan-si, Gyeongbuk 712-749, South Korea

Supporting Information

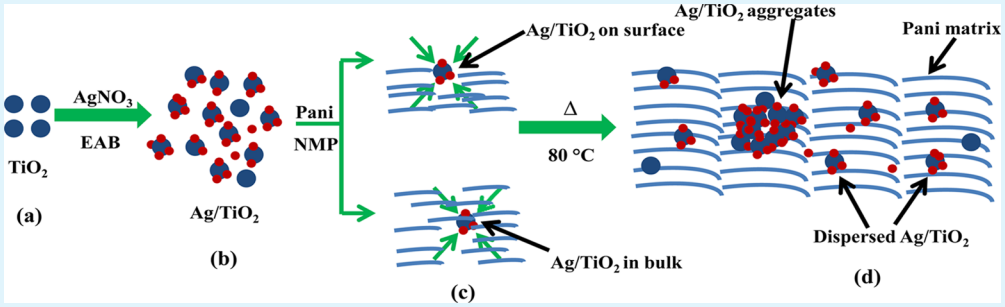

ABSTRACT: The development of organic−inorganic photoactive materials has resulted in significant advancements in heterogeneous visible light photocatalysis. This paper reports the synthesis of visible light-active Ag/TiO_2@Pani nanocomposite film via a simple biogenic−chemical route. Electrically conducting Ag/TiO_2@Pani nanocomposites were prepared by incorporating Ag/TiO_2 in *N*-methyl-2-pyrrolidone solution of polyaniline (Pani), followed by the preparation of Ag/TiO_2@Pani nanocomposite film using solution casting technique. The synthesized Ag/TiO_2@Pani nanocomposite was confirmed by UV−visible spectroscopy, photoluminescence spectroscopy, scanning electron microscopy, X-ray diffraction, X-ray photoelectron spectroscopy, and thermogravimetric analysis. The Ag/TiO_2@Pani nanocomposite film showed superior activity towards the photodegradation of methylene blue under visible light compared to Pani film, even after repeated use. Studies on the thermoelectrical behavior by DC electrical conductivity retention under cyclic aging techniques showed that the Ag/TiO_2@Pani nanocomposite film possessed a high combination of electrical conductivity and thermal stability. Because of its better thermoelectric performance and photodegradation properties, such materials might be a suitable advancement in the field of smart materials in near future.

KEYWORDS: *polyaniline, nanocomposites, Ag/TiO_2@Pani, photocatalysis, visible light active, cyclic stability*

INTRODUCTION

Since the first report in Nature in 1972, research in the field of photocatalytic active semiconducting metal oxides has advanced considerably.[1] Among the different metal oxides, TiO_2 has been the most promising and well-studied over the years because of its photocatalytic properties owing to its wide band gap, high chemical stability, large surface area, non-toxicity, and wide commercial availability.[2−4] On the other hand, the wide band gap (3.2 eV) of TiO_2 limits its utilization under visible light irradiation, which comprises a large part of the solar spectrum. To overcome this problem, band gap engineering has been carried out to improve the utilization of solar light using a range of techniques, such as metal ion doping,[5−7] nonmetal doping,[8−10] noble metal deposition,[11] narrow band gap semiconductors coupling,[12] dye sensitization,[13] and polymer composites formation.[14] Among the different techniques, metal doping has been the most commonly used approach for achieving visible light-driven photocatalysis of TiO_2 because of its simplicity, high efficiency and facile synthesis.

Noble metals exhibit enhanced photocatalytic activity as they can strongly absorb visible light because of their surface plasmon resonance and can also work as electron traps to activate the reaction sites.[15] Therefore, it is expected that doping with noble metals, such as Ag or Au with TiO_2, to form Au or Ag/TiO_2 photocatalyst can be an efficient way of achieving visible light-driven photocatalysis of TiO_2. In view of the above possibilities, many workers have reported the production of nanocomposites of TiO_2 and ZnO with noble metals to enhance the photocatalytic properties of the semiconductor.[16−18] On the other hand, the synthetic method

Received: January 23, 2014
Accepted: May 16, 2014
Published: May 16, 2014

employed, often suffer from the following limitations, that is, use of hazardous chemicals, capping agents, etc. To overcome these limitations, our group has used a greener route for the synthesis of Ag/TiO_2 nanocomposites using an electrochemically active biofilm (EAB)[3,19,20] and reported the highly efficient degradation of 4-nitrophenol, methylene blue (MB), and methyl orange under visible light activity.[3,21] The EABs are well known in microbial fuel cells and bioinspired nanomaterial synthesis. In this study, EABs was used as a biogenic tool, where we have utilized living microorganisms for the synthesis of Ag/TiO_2 nanocomposite. As the amount of photocatalyst used is generally in milligrams, the recovery of catalyst is a tedious job, which in turn affects its reproducibility. Several studies have shown that a catalyst supported on a substrate not only solves the recovery problems but also affects the efficiency because of the synergism between the constituents. Robert et al.[22] reported that TiO_2 supported on glass-fibers is stable, even after several uses. Similarly, Chang-Soo Lee et al.[23] developed TiO_2 thin films on a polymer substrate with high catalytic activity. Among the different polymer substrates, polyaniline (Pani) is exciting because of its low cost, high stability, and ease of synthesis.[24] In addition, it enhances the photocatalytic property of metal oxides because of the synergism between the constituents.[25]

Therefore, Pani-modified, metal-doped TiO_2 might be an exciting area of research because the resulting Pani nanocomposite is expected to have unique properties, such as enhanced photo catalytic activity, high stability, etc., because of the synergism between the constituents. Accordingly, this paper reports Ag/TiO_2@Pani nanocomposite film by the in-situ oxidative polymerization of aniline in the presence of Ag-modified TiO_2. The prepared nanocomposite was used for the degradation of MB dye under visible light irradiation. The electrical conductivity and electrical stability of Pani and Ag/TiO_2@Pani nanocomposite film was also evaluated and the latter showed higher conductivity and better stability than Pani film.

EXPERIMENTAL SECTION

Chemicals and Instrumentation. Aniline, silver nitrate ($AgNO_3$, 99%), methylene blue (MB), *N*-methyl-2-pyrrolidone (NMP) and TiO_2 (average particle size ~21 nm) were purchased from Sigma-Aldrich. Potassium persulfate (PPS), HCl, NH_4OH, and methanol were obtained from Duksan pure chemicals, Korea, and used as received. The water used in these experiments was de-ionized water obtained using a PURE ROUP 30 water purification system.

X-ray diffraction (XRD, PANalytical, X'Pert-PRO MPD) was performed using Cu Kα radiation (λ = 0.15405 nm). The surface morphology was examined by scanning electron microscopy (SEM, Hitachi-4800). The UV–visible diffuse absorbance and reflectance spectra (DRS) were measured using a UV–vis–NIR spectrophotometer (VARIAN, Cary 5000 U.S.A.). Thermogravimetric analysis (TGA) and differential thermal analysis (DTA) was performed by using a Perkin Elmer (Pyris Dimond) instrument heating from ~25 to ~800 °C at the rate of 10 °C min^{-1} at a N_2 flow rate of 200 mL/min. X-ray energy photoelectron spectroscopy (XPS, ESCALAB 250) was performed using a monochromatized Al Kα X-ray source ($h\nu$ = 1486.6 eV) with a 500 μm spot size, at Korea Basic Science Institute (KBSI). The photoluminescence (PL) of the samples was recorded by using Kimon, 1 K, Japan spectroscope, at KBSI. The photocatalytic degradation and photoelectrochemical experiments, such as electrochemical impedance spectroscopy (EIS) and linear sweep voltammetry (LSV), were conducted using a 400 W lamp (λ > 400 nm) with an irradiation intensity of 31.0 mW cm^{-2} (3M, USA). The EIS and LSV measurements were carried out using a potentiostat (Versa STAT 3, Princeton Research, USA) with a standard three-electrode system in a 0.2 M Na_2SO_4 solution as the electrolyte. In this system, Ag/AgCl (saturated with KCl), a Pt gauge and Pani or Ag/TiO_2@Pani film were used as the reference, counter and working electrodes, respectively. All measurements of the DC electrical conductivity (σ) were performed using a 4-in-line probe electrical conductivity measuring instrument with a PID controlled oven (Scientific Equipment, Roorkee, India). The calculations were performed using the following equation:

$$\sigma = [\ln 2(2S/W)]/[2\pi S(V/I)] \quad (1)$$

where I, V, W, and S are the current (A), voltage (V), thickness of the film (cm), and probe spacing (cm), respectively, and σ is the DC electrical conductivity (S/cm).[26]

Preparation of Ag/TiO_2@Pani Nanocomposite Film. The preparation of Ag/TiO_2@Pani was carried out in two steps: the synthesis of Ag/TiO_2 followed by its incorporation into Pani to prepare Ag/TiO_2@Pani nanocomposite film. The synthesis of Ag/TiO_2 is reported elsewhere.[3,27] The nanocomposite system of Ag/TiO_2 and Pani was prepared by mixing the emeraldine base of Pani (Pani-EB) with Ag/TiO_2. The synthesis of Pani-EB is reported elsewhere.[26] In a typical process, Pani-EB was first dissolved in 50 mL of NMP with continuous stirring for 24 h for complete dissolution. The EAB-assisted Ag/TiO_2 (3 wt % of Pani-EB) was mixed slowly with Pani solution under continuous stirring and occasional shaking in an ultrasonic bath for few minutes for proper dispersion of Ag/TiO_2 inside the NMP solution of Pani. Later, the Ag/TiO_2@Pani nanocomposite film was prepared using solution casting technique. For the DC electrical conductivity, photoelectrochemical and photocatalytic studies, the Pani and Ag/TiO_2@Pani nanocomposite films were doped in 100 mL of a 1 M HCl solution followed by washing with double distilled water and drying at 60 °C for 24 h.

Studies and Measurement. The electrical conductivity of the Ag/TiO_2@Pani nanocomposite film was measured by 4-in-line probe electrical conductivity measuring instrument. The stability of the nanocomposites was examined in terms of the retention of their DC electrical conductivity under cyclic aging conditions. In the cyclic aging experiments, the DC electrical conductivity was measured at temperatures ranging from 40 to 150 °C five times at 45 min intervals. The Ag/TiO_2@Pani nanocomposite film was also used for the degradation of MB under visible light irradiation. Details of the experimental setup are reported elsewhere.[21]

RESULTS AND DISCUSSION

A simple biogenic–chemical route was used for the synthesis of Ag-modified TiO_2 and later its composite with Pani. A unique protocol of EAB-assisted synthesis was used to prepare Ag/TiO_2.[3,20,27] The advantage of this synthetic method is that it does not involve the use of hazardous chemicals, capping agents, etc. Moreover, the entire reaction takes place in water. Pani was used as a supporting matrix for the preparation of Ag/TiO_2@Pani nanocomposites which exhibited enhanced electrical conductivity and visible light activity compared to Pani. Moreover, the Ag/TiO_2@Pani nanocomposite film showed promising prospects as a visible light active photocatalyst, which can be used repeatedly for photodegradation, and solved the problems generally faced in the case of a powder catalyst, where the recovery of the catalyst is a major problem.

Scanning Electron Microscopy. Figure 1 presents SEM images of the Pani and Ag/TiO_2@Pani film. Figure 1a shows that the Pani matrix provides a smooth platform for the anchoring of Ag/TiO_2 (the morphology of Ag/TiO_2 can be seen from Supporting Information Figures S1 and S2). The Ag/TiO_2 nanocomposite is distributed in the form of agglomerates with Pani because of the nucleation effect of Ag/TiO_2, giving flaky or tremella like morphology at different regions of film while regions with little or no Ag/TiO_2 showed smooth morphology similar to pure Pani film. Similar flaky/

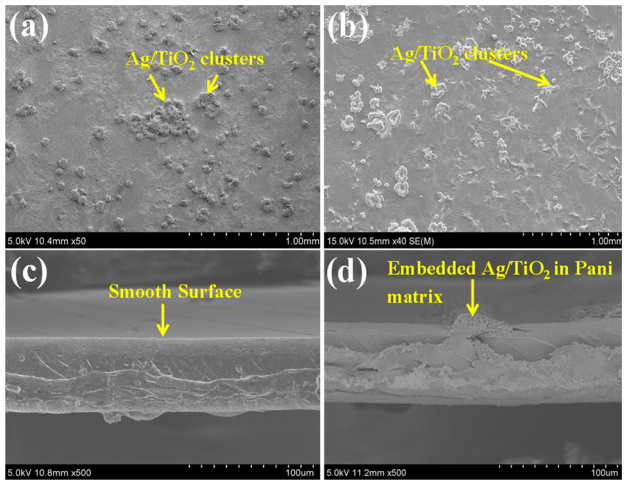

Figure 1. SEM images of (a) as-prepared Ag/TiO_2@Pani, (b) Ag/TiO_2@Pani after degradation of MB, (c) fractured side view of the Pani film, and (d) fractured side view of Ag/TiO_2@Pani nanocomposite film.

tremella like morphology has also been reported by Pang et al.[28] in the case of V_2O_5@Pani nanocomposite nanosheets. SEM revealed the surface and embedded Ag/TiO_2 nanoparticles, Figure 1c and 1d corresponds to the fractured view of Pani and Ag/TiO_2@Pani nanocomposite film, respectively. The morphology of Ag/TiO_2@Pani nanocomposite film is entirely different from pure Pani film. Ag/TiO_2 clusters on the surface are well dispersed inside the Pani matrix, as evident from the fractured view, which is beneficial for translating the properties of Ag/TiO_2 and Pani into Ag/TiO_2@Pani nanocomposite system (Supporting Information Figure S3). Figure 1b shows the SEM image of Ag/TiO_2@Pani nanocomposite film after the degradation of MB. The morphology was not affected significantly after dye degradation indicating that Ag/TiO_2 was anchored strongly to the Pani matrix with little or no loss, suggesting the applicability of Ag/TiO_2@Pani nanocomposite film for repeated use.

Aggregation/Dispersion Behavior of Ag/TiO_2 Inside Ag/TiO_2@Pani Film. The nanocomposite of Ag/TiO_2@Pani was prepared by dispersing Ag/TiO_2 in Pani solution (made in NMP), and later using solution casting technique to prepare thin free standing film of Ag/TiO_2@Pani nanocomposite. The Ag/TiO_2@Pani film was not smooth, which might be due to the aggregation of Ag/TiO_2 in different regions of the film (Figure 2), while the Pani film showed smooth surface morphology. Therefore, the major obstacle to the widespread use of Ag/TiO_2 with Pani is its poor wettability and tendency to rope up in the solvents, which is similar to the aggregation behavior of the CNT@Pani film, as reported earlier.[29] Ag/TiO_2 exists as ropes or bundles because of the high van der Waal forces, which become entangled in the solid state to form a highly dense and complex structure, which is extremely resistant to wetting.

The nucleation behavior of Ag/TiO_2 can also be explained based on the nucleation theory of solids in liquids. The physicochemical properties of Pani are largely affected by the confinement of Ag/TiO_2 in different areas of the Pani matrix. This aggregation phenomenon depends strongly on the $Ag/TiO_2\cdots Ag/TiO_2$ and $Pani\cdots Ag/TiO_2$ interactions.[30] In terms of the interaction between Pani and Ag/TiO_2, there are two types of forces, that is, adhesive forces (between Pani and Ag/TiO_2) and cohesive forces (between Ag/TiO_2 and Ag/TiO_2). One possible explanation might be the cohesive force between the clustering molecules, which is certainly higher than the adhesive force between the Pani matrix and Ag/TiO_2. As these forces are highly unbalanced, it gives rise to the very poor wetting of Ag/TiO_2 by the Pani matrix. The Ag/TiO_2 on the surface has more surface energy than those in the bulk due to unbalanced nature of the forces experienced by the molecules on the surface, as shown in Figure 2c. The migration and aggregation of Ag/TiO_2 particles might be driven by the instability of the nanoparticles because of their high surface free energy, and their aggregation would produce thermodynamically stable clusters.[31] The preferred sites for the aggregation of Ag/TiO_2 are the phase boundary, where the effective surface energy is lower, which causes a decrease in the free energy barrier, thereby enhancing the nucleation process. SEM showed that the size of the Ag/TiO_2 clusters increased to a certain critical size as the total free energy change reached maximum at a critical size. After this point, it decreases continuously to favor the stabilization and growth of the aggregate formation of Ag/TiO_2 on to the Pani matrix.[32]

The aggregate formation behavior can be interpreted as interplay between particle-particle clustering and particle–substrate attraction, which is governed largely by the Pani matrix.[33] The rate of nucleation, which is the reason for the aggregation of the Ag/TiO_2 into the Pani matrix can be expressed mathematically using the following mathematic model.[34]

The rate of nucleation J is proportional to the probability of forming solid nuclei with excess energy, ΔG^*, which is expressed as follows:

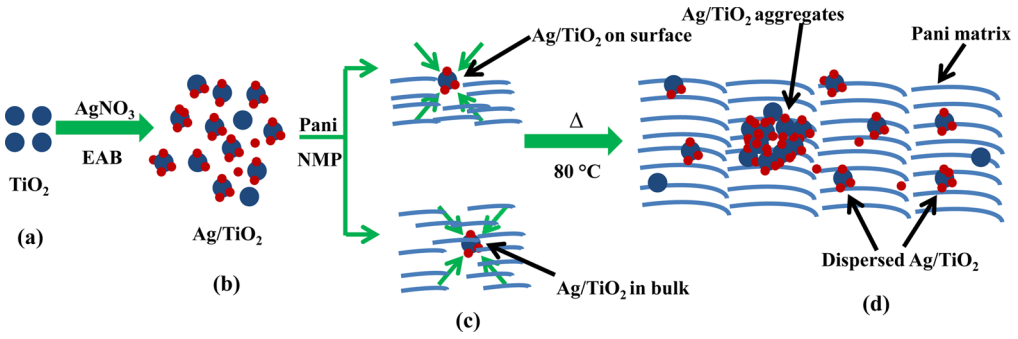

Figure 2. Schematic diagram of the preparation of Ag/TiO_2@Pani nanocomposite film. Panel c shows the balanced and unbalanced forces acting on Ag/TiO_2 in the bulk and on the surface, respectively.

dx.doi.org/10.1021/am500488e | ACS Appl. Mater. Interfaces 2014, 6, 8124–8133

$$J = J_0 \exp(-\Delta G^*/kT) \quad (2)$$

where k is Boltzmann's constant and the pre-exponential factor J_0 depends upon the density of available nucleation sites. In classical heterogeneous nucleation theory,[35] the energy barrier, ΔG^*, is given by

$$\Delta G^* = 16\pi\gamma^3 f(\theta)/3\Delta G^2 \quad (3)$$

Equation 2 relates to the rate of nucleation and surface energy of the solid nuclei and eq 3 relates the energy barrier and surface energy of the molecule. Nucleation starts when this energy barrier or threshold is achieved. Lower the threshold, easier will be the nucleation and aggregation. Thus, it can be explained that possible way to decrease Ag/TiO_2 agglomerates is by increasing the surface area of Ag/TiO_2 nanocomposite. As with the enhancement of the surface area the barrier or threshold also increases consequently unfavoring the nucleation and stopping the aggregation.

X-ray Diffraction. Figure 3 shows XRD patterns of the Pani and Ag/TiO_2@Pani nanocomposite films. In case of Pani, a broad amorphous peak observed at 19.51° 2θ was assigned to the periodicity parallel to the polymer chain.[36] XRD of Ag/TiO_2@Pani indicated that the nanocomposite is crystalline and showed a XRD peak for Pani at 19.51° 2θ, as well as XRD peaks for TiO_2, as reported elsewhere.[3] Clear anatase and rutile phases of TiO_2 as well as Ag were observed without other detectable impurities. All XRD peaks corresponding to TiO_2 and Ag were well indexed to the tetragonal and face-centered cubic structures, respectively. The peaks of all constituents are indicated with their corresponding (hkl) parameters. These results suggest that TiO_2 and Ag are coexistent in the samples as two different and distinct materials with no interdiffusion. In addition, a thorough examination of the XRD patterns of the TiO_2 revealed anatase and rutile. The XRD patterns of anatase TiO_2 nanoparticles indicated that the position and intensity of the characteristic peaks of the samples were confirmed with the JCPDS file No. 73-1764. The rutile phase appeared in the XRD peaks and was confirmed by the JCPDS file No. 76-318. All the peaks of Ag in Figure 3 were assigned to the diffraction of the planes of face-centered cubic Ag (JCPDS file No. 04-0783). The relative abundance of anatase to rutile was calculated from the following equation:[37]

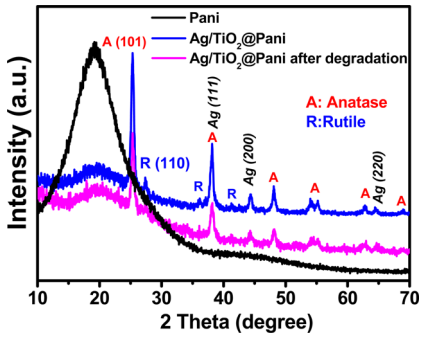

Figure 3. XRD patterns of Pani and Ag/TiO_2@Pani nanocomposite film before and after MB degradation.

$$F_R = 1.26I_R/(I_A + 1.26I_R) \quad (4)$$

where I_R and I_A are the strongest intensities of rutile (110) and anatase (101) peaks, respectively. The calculated phase percentages of the constituent anatase and rutile phases were approximately equal to 80% and 20 %, respectively. To analyze the XRD patterns, the crystal structure was refined using the Rietveld profile fitting technique.[38] The refinement was performed, assuming a tetragonal structure with the $I41/amd$ space group (SG No. 141) for anatase, and the $P42/mnm$ space group (S.G no 136) for rutile. The observed and calculated patterns are in good agreement with each other. Supporting Information Table S1 shows all the lattice parameters obtained from the Rietveld refinement.

The maximum intensities of peak (101) for anatase, (110) for rutile, and (111) for Ag were used to quantify the crystallite sizes of TiO_2 and Ag. The mean crystallite sizes were estimated using the full width at half maxima of the XRD peaks. Using the Scherrer formula,[39] the expression for the full width at half maximum of the XRD peaks can be expressed as

$$\beta_{Size} = \kappa\lambda/t \cos\theta \quad (5)$$

where κ is the grain shape factor (0.89 for spherical), λ is the wavelength of CuK_α (1.5406 Å) and t is the thickness of the crystal and θ is the Bragg's angle. The mean crystallite sizes of the anatase and rutile phases of TiO_2 as well as Ag were ~16, 23, and 6 nm, respectively (Supporting Information Table S1). To examine the impact of dye degradation on Ag/TiO_2@Pani, the XRD patterns were also measured after the degradation of MB. The XRD patterns before and after the degradation of MB were similar, suggesting that the degradation experiments has little or no impact on the Ag/TiO_2@Pani nanocomposite film and thus the film can be used repeatedly.

Diffuse Reflectance/Absorbance Spectroscopy. The UV-vis diffuse absorbance spectra (Figure 4) and DRS (Supporting Information Figure S4) of Pani revealed two absorption peaks at 268 and 495 nm, which were assigned to a $\pi-\pi$ transition of the benzenoid rings and charge transfer from the benzenoid to the quinoid, respectively. In the case of Ag/TiO_2@Pani, the peaks were blue shifted, which indicates the coordination of Ag/TiO_2 with a nitrogen atom, and a permitted interaction with each other via the π-conjugated system was observed. The blue shift upon the addition of Ag/TiO_2 is consistent with previous work in the case of Pd@Pani nanocomposites, where a blue shift occured after the addition of Pd nanoparticles.[40]

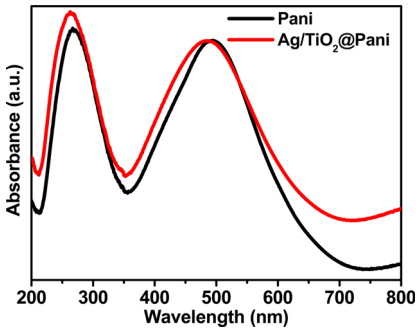

Figure 4. UV–vis diffuse absorbance spectra of Pani and the Ag/TiO_2@Pani nanocomposite film.

X-ray Photoelectron Spectroscopy. The surface characterization and chemical states of Ag/TiO_2 and Ag/TiO_2@Pani nanocomposite film was examined by XPS. The XPS survey scan of Ag/TiO_2 revealed the presence of C, Ag, O, and Ti, whereas in the case of Ag/TiO_2@Pani, in addition to these elements, N was also detected (Supporting Information Figure

S5a). The peak in Supporting Information Figure S5(b) (C 1s = 284.6 eV) was assigned to residual carbon from the sample and hydrocarbons from the XPS instrument. Figure 5a presents

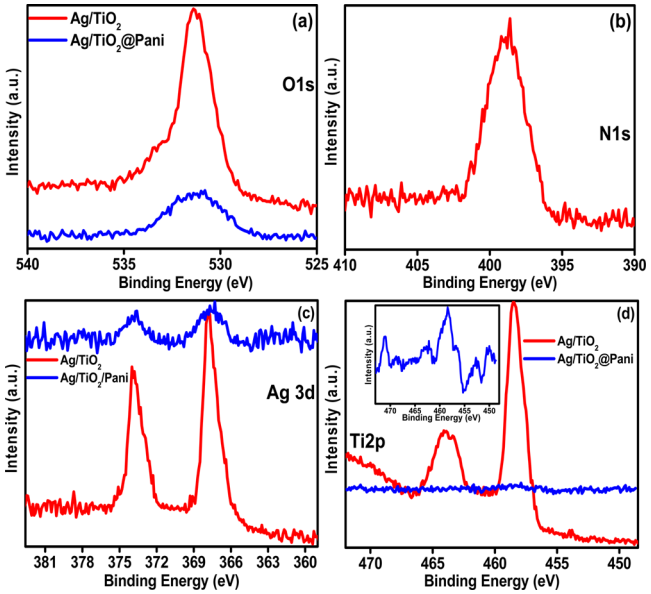

Figure 5. XP spectra of the Ag/TiO_2 and Ag/TiO_2@Pani nanocomposites film for (a) O 1s peaks, (b) N 1s peaks of Ag/TiO_2@Pani (c) Ag 3d peaks, and (d) Ti 2p peaks. The inset in 5 (d) shows Ti 2p peaks of the Ag/TiO_2@Pani film.

the O 1s spectra of Ag/TiO_2 and Ag/TiO_2@Pani. The peak was assigned to the O bonds, such as Ti−O−Ti and Ti−O−H.[41] The slight change in the binding energy of O 1s from 531.30 to 531.28 eV in the case of Ag/TiO_2 and Ag/TiO_2@Pani, respectively, is probably due to the strong interactions between the oxygen of TiO_2 and imine nitrogen. The N 1s peak at 402.6 eV in Figure 5(b) corresponds to positively quinoid amine and benzenoid amine, which is consistent with the structure of Pani as reported by Mac Diarmid et al.[42]

Figure 5c presents the core level Ag 3d spectra of the Ag/TiO_2 (367.73 eV) and Ag/TiO_2@Pani (367.63) nanocomposite. Figure 5(d) presents the Ti 2p spectra of Ag/TiO_2 (458.39 eV) and Ag/TiO_2@Pani (458.13 eV) nanocomposites. In the case of Ag/TiO_2@Pani, the peaks for Ag and Ti were diffused significantly, which might be due to the encapsulation of Ag/TiO_2 inside the Pani matrix. Moreover, the existence of Ti 2p peak in Ag/TiO_2@Pani is also shown in Supporting Information Figure S5c and in the inset of Figure 5d for clarity. A slight shift (decrease) in the binding energy of Ag 3d (0.10 eV) and Ti 2p (0.26 eV) in Ag/TiO_2@Pani was observed, which was assigned to the interaction of Ag/TiO_2 with Pani, probably via coordination between the imine nitrogen and titanium.[43,26]

Photoluminescence Studies. To examine the optical properties, a PL study of Ag/TiO_2, Pani, and Ag/TiO_2@Pani were carried out. PL can be exploited to understand the fate of e^-/h^+ pairs, the efficiency of charge carrier trapping, and migration in materials. The PL spectra can be decomposed into several bands that are associated with different radiative recombination processes of the charged carriers produced by band−band irradiation.[44] Figure 6 presents the PL spectra for the different samples. In the case of Ag/TiO_2, there was a shift in the emission peak from ∼518 nm (for pure TiO_2) to ∼455

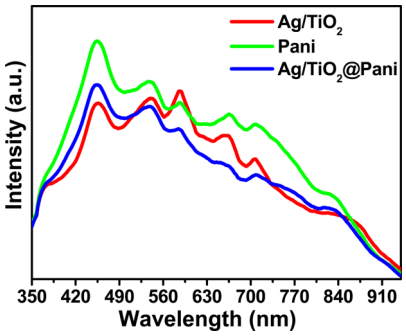

Figure 6. PL spectra of Ag/TiO_2, Pani, and Ag/TiO_2@Pani nanocomposite films.

nm, which might be the result of the transition related to free exciton O_2^- to Ti_4^+ charge transfer.[3] The peaks from 450−500 nm were assigned to free electrons recombination from the conduction band to the recombination center at the ground state. In the case of Ag/TiO_2@Pani, the emission peak at ∼450 nm is slightly higher or comparable in intensity to Ag/TiO_2 while the intensity decreases with the increase in wavelength and the peak at ∼540 nm had lower intensity, indicating slightly lower recombination rate of electrons than Ag/TiO_2. This suggests that the photo-induced electrons and holes are trapped by the synergistic effect in the Ag 3d energy level and by Pani, which improves the separation and suppresses the automatic recombination process of photogenerated electrons and holes in Ag/TiO_2@Pani compared to Pani and Ag/TiO_2. In other words, weaker the excitonic PL spectra, the higher the separation rate of the photo-induced charge carriers, which will favor the photocatalytic activity.[45]

Thermogravimetric Analysis. TGA was used to examine the thermal stability of the Ag/TiO_2@Pani nanocomposite film compared to the Pani film. Pani and Ag/TiO_2@Pani nanocomposite followed similar weight loss pattern in the three major stages of weight loss. The first weight loss until ∼150 °C was attributed to the loss of water and other volatile impurities. The weight loss from ∼150 to 400 °C was assigned to the removal of higher oligomers and residual NMP.[26] The degradation curve revealed massive weight loss because of thermo-oxidative decomposition of Pani, which occurs in the temperature range of ∼400−550°C.[46] The DTA curve showed a sharp peak at ∼510 and ∼525 °C for Pani and Ag/TiO_2@Pani, respectively. Thus, it can be interpreted that Ag/TiO_2 has some stabilizing interaction with Pani, hence an increase in the stability (Figure 7). The weight loss due to the decomposition of Pani and Ag/TiO_2@Pani involves the evolution of degradation products, such as ammonia, aniline, p-phenylenediamine, *N*-phenylaniline, *N*-phenyl-1,4-benzenediamine, carbazole, pyridine-based heterocycle, methane, acetylene, etc.[26]

The activation energy (E_a) for the thermo-oxidative degradation of the materials was evaluated using the well-known integral method reported by Broido.[47,48] According to the Broido eqs 6 and 7,

$$\ln\left[\ln\left(\frac{1}{y}\right)\right] = -\frac{E_a}{RT} + c \tag{6}$$

$$Y = (w_t - w_\infty)/(w_0 - w_\infty) \tag{7}$$

dx.doi.org/10.1021/am500488e | ACS Appl. Mater. Interfaces 2014, 6, 8124−8133

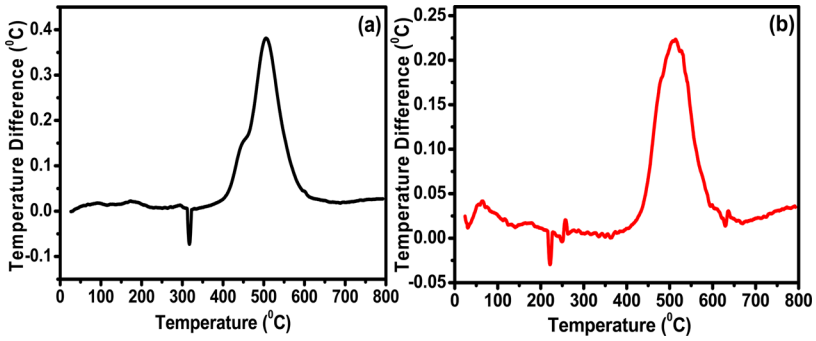

Figure 7. DTA of (a) Pani and (b) Ag/TiO_2@Pani nanocomposite film.

where Y is the fraction of the samples not yet decomposed, w_0 and w_∞ are the initial and final weight, and w_t is the weight at a particular time. The activation energy (E_a) for the degradation process was derived from the slope of the plots (as shown in Supporting Information Figure S6) of $\ln[\ln(1/Y)]$ vs $1000/T$ (K^{-1}). From the DTA curve, it can be seen that degradation of Pani takes place at ~510 and for Ag/TiO_2@Pani, the degradation stars at ~525 °C. Thus, the activation energy was calculated for that region. The activation energies of Pani and Ag/TiO_2@Pani were found to be 30.21 and 34.86 kJ/mol, respectively. It should be taken into account that Ag/TiO_2@Pani is a multicomponent system and there are multiple factors that should be considered. The system cannot be considered a linear process, the first part was until ~500 °C and the later part started from 500 to 800 °C, whereas degradation of the Pani backbone occurred. These two parts of the degradation process are strongly dependent on (a) interaction of Ag/TiO_2 between the Pani chains and (b) thermal stability of Ag/TiO_2, and these two processes compete with each other.

TGA suggests that initially, the weight loss until ~500 °C in the case of Ag/TiO_2@Pani is higher in comparison to Pani. However, from 500 °C onwards, the weight loss for Pani and Ag/TiO_2@Pani were found to be ~40% and 28%, respectively (Figure 8). Kumar et al.[46] in their Cu@Pani and Cu_2O@Pani

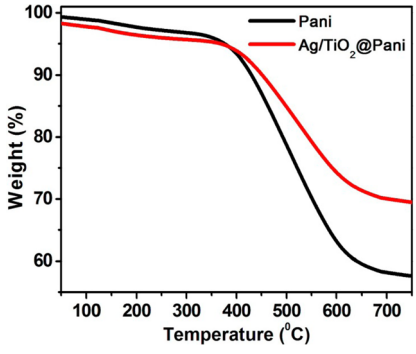

Figure 8. TGA of the Pani and Ag/TiO_2@Pani nanocomposite films.

composites showed that the perturbation of the nanomaterials affects the three dimensional structure of the polymer, which might weaken the van der Waal's interactions between the polymer chains, thereby affecting the stability of the polymer. In the light of his observations, it can be interpreted that the interaction between Pani and Ag/TiO_2 may affect the three-dimensional Pani structure, thereby initially triggering greater weight loss until ~500 °C. Another factor is the higher thermal stability of Ag/TiO_2 in comparison to Pani, which requires much higher temperature for degradation.[49] Thus, the stabilization effect of Ag/TiO_2 dominates at higher temperature and contributes for the stability above 500 °C.

Electrical Conductivity. The DC electrical conductivity of HCl doped Pani and Ag/TiO_2@Pani nanocomposite film was measured using a 4-in-line probe technique. The electrical conductivity showed an increase from 4.59 S/cm to 5.45 S/cm after loading with Ag/TiO_2. Nagaraja et al.[50] in their *p*TSA doped TiO_2@Pani nanocomposite reported that the addition of TiO_2 increases the compactness of the sample, causing greater coupling through the grain boundaries, which in turn enhances the electrical conductivity. This suggests that in the Ag/TiO_2@Pani nanocomposite film, Ag/TiO_2 leads to a decrease in the conjugated lengths in the Pani chains. In addition, a small number of nanoparticles are believed to act as a more efficient network for charge transport, by hopping or tunneling, resulting in an increase in the electrical conductivity.[43]

Pani and Ag/TiO_2@Pani nanocomposite films were also studied for DC electrical conductivity retention under cyclic aging conditions (Supporting Information Table S2). Pani and the Ag/TiO_2@Pani nanocomposite film showed an increase in electrical conductivity at higher temperatures, which is normal thermal activation behavior. The subsequent cycle showed similar loss behavior but the Ag/TiO_2@Pani film showed greater retention (21.46% compared to 13.29% in the case of Pani) in the DC electrical conductivity than Pani. The increase or decrease in the electrical conductivity of the doped nanocomposite film during the cyclic aging experiment might be due to various competing factors. The increase in electrical conductivity might be attributed to, for example, (1) the doping by H^+ ions of acid, (2) the annealing effect during heating/cyclic aging conditions, (3) the presence of trapped moisture in the film, (4) the plasticizing effect of any traces of solvent (NMP) present, (5) the high electrical conductivity of Ag, and (6) elevation of temperature because of an increase in the number of charge-carriers, etc. The decrease in electrical conductivity might be attributed to, for example, (1) the removal of H^+ ions of the acid, (2) the poor electrical conductivity of TiO_2, (3) the removal of trapped moisture in the nanocomposite film at high temperatures, and (4) degradation of the conducting polymer at elevated temperature etc.[26]

Photoelectrochemical Studies. Figure 9a shows the EIS Nyquist plots of the Pani and Ag/TiO_2@Pani nanocomposite film in dark and under visible light irradiation. The EIS Nyquist plot showed the arc radius of the Ag/TiO_2@Pani nanocomposite film, which was smaller than that of the Pani film. The arc radii of the Ag/TiO_2@Pani photocatalysts were smaller than those of Pani in the cases of dark and under visible light

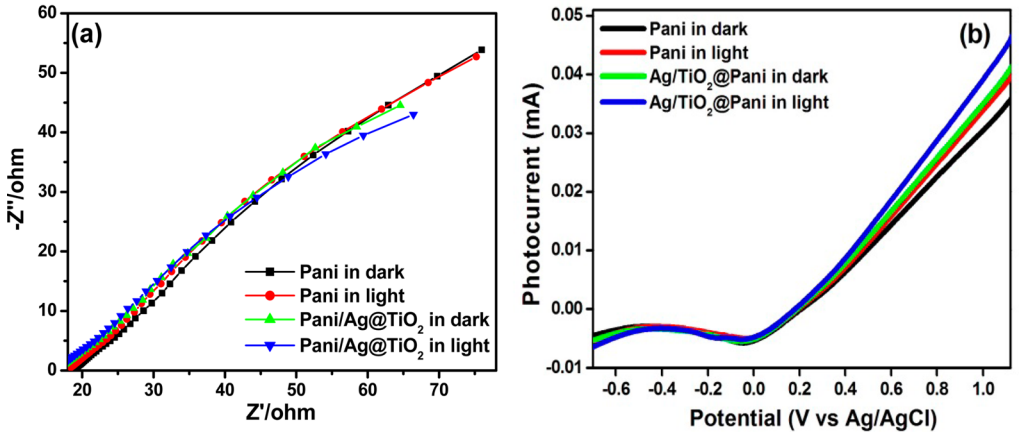

Figure 9. (a) EIS (Nyquist plots), and (b) LSV spectra of Pani and Ag/TiO_2@Pani nanocomposite film in dark and under visible light irradiation.

irradiation. This suggests that the Ag/TiO_2@Pani photocatalysts have lower resistance than the Pani, which can accelerate the interfacial charge-transfer process. This also shows that the more effective separation of photogenerated electron hole pairs and faster interfacial charge transfer occurred in the Ag/TiO_2@Pani nanocomposite film.[21,51,52] This confirmed that the Ag/TiO_2@Pani photocatalyst has the lowest charge transfer resistance and is most suitable for photocatalytic applications. These enhanced photoelectric characteristics suggest that the interfacial interaction of Ag/TiO_2 and Pani can effectively improve the photocatalytic efficiency of Pani.

To examine the possible mechanisms for the enhanced visible light photoactivity (i.e., photocurrent), LSV for Ag/TiO_2@Pani and Pani films were performed in dark and under visible light irradiation.[52] Photocurrent measurements can be useful to understand the synergistic effect of the individual components (Ag/TiO_2 and Pani) of the nanocomposite materials.[53] Figure 9b shows the photoresponse of Ag/TiO_2@Pani and Pani in dark and under visible light irradiation. The photocurrent of the Ag/TiO_2@Pani film was improved compared to the Pani film. Ag/TiO_2@Pani showed higher photocurrent than Pani under the same conditions, suggesting that the Ag/TiO_2@Pani exhibited stronger ability for the separation of electron−hole pairs than Pani, as also revealed by PL analysis. An improvement in the photocurrent for Ag/TiO_2@Pani showed that it can be motivated easily by visible light, thereby producing more photoinduced carriers, resulting in higher visible photocatalytic activity. Similar trends have also been previously reported.[3,53] This suggests that the separation efficiency of photoinduced electrons and holes was enhanced considerably through the synergistic effect of Ag/TiO_2 and Pani.

Visible Light Photocatalytic Activities of Ag/TiO_2@Pani and Pani. Supporting Information Figure S7 shows the photocatalytic activity of the Pani and Ag/TiO_2@Pani under visible light irradiation, which indicates the photodegradation efficiency of Ag/TiO_2@Pani for the degradation of MB.[3,21,52] The performance of Ag/TiO_2@Pani film was significantly higher than that of the Pani film.

Furthermore, the photocatalytic degradation kinetics of MB by Pani and Ag/TiO_2@Pani film was calculated by equation reported elsewhere[3,54] and the result is shown in Figure 10. The rate constant (k) of the Pani and Ag/TiO_2@Pani for the degradation of MB were found to be 0.0406/h (R^2 = 0.9516) and 0.2695/h (R^2 = 0.9537), respectively. The k value of the Ag/TiO_2@Pani showed ~7 times higher visible light degradation of MB than Pani. Figure 11 shows the mechanism for the photo generation of charge carriers on the surface of the Ag/TiO_2@Pani photocatalyst.

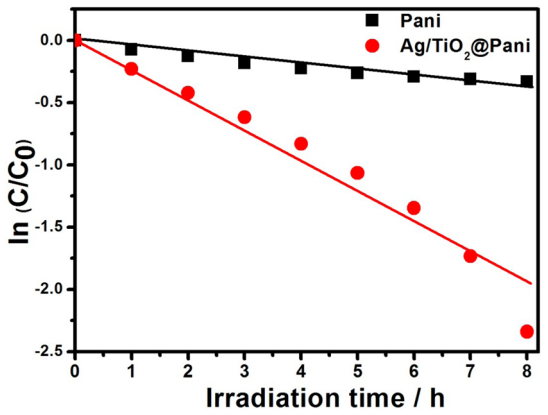

Figure 10. Plot of ln C/C_0 vs the irradiation time (h) for the photodegradation of MB by Pani and Ag/TiO_2@Pani nanocomposite film.

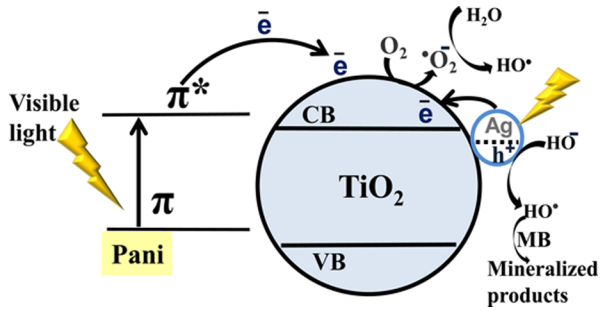

Figure 11. Proposed mechanism for the degradation of MB by the Ag/TiO_2@Pani nanocomposite film.

Under visible light irradiation, Pani absorbs light to induce a $\pi \rightarrow \pi$ transition, transporting the excited-state electrons to the π orbital. These excited-state electrons are readily injected into the conduction band of TiO_2, are subsequently transferred to the surface, and react with adsorbed water and oxygen to yield hydroxyl and superoxide radicals.[55] Furthermore, during visible light irradiation, the equilibrated Fermi level electrons of Ag are

injected rapidly into the TiO_2 conduction band via a surface plasmon resonance (SPR) mechanism (Figure 11).[3,56−61] These injected electrons are trapped by adsorbed oxygen/water molecules on Ag/TiO_2 to yield hydroxyl and superoxide radicals.[58,59] Therefore, large amounts of oxidative radical formation are responsible for enhanced photocatalytic activity of Ag/TiO_2@Pani photocatalyst. Because of the synergy between Ag/TiO_2 and Pani, rapid photogenerated charge separation and relatively slow charge recombination enhances the photocatalytic activity of the Ag/TiO_2@Pani photocatalyst significantly.

CONCLUSIONS

Ag/TiO_2@Pani nanocomposite film was prepared successfully via a simple biogenic-chemical route. The nanocomposite film was also studied for the thermoelectric behavior. The Ag/TiO_2@Pani nanocomposite film showed higher conductivity (5.45 S/cm) than Pani film (4.59 S/cm) due to the high mobility of charge carrier and the presence of Ag/TiO_2. The Ag/TiO_2@Pani nanocomposite film examined under cyclic aging conditions showed more retention of the DC electrical conductivity than Pani film. The nanocomposite film showed superior visible light photocatalytic activity in the decomposition of MB than Pani. The recycling test showed that the Ag/TiO_2@Pani nanocomposite film can be used repeatedly without much loss in visible light activity, which is advantageous compared to the powder photocatalyst, where the recovery of catalyst is a tedious job. The high photocatalytic activity can be attributed to the synergistic effect originating from the excited state electrons, which are injected readily into the conduction band of TiO_2. These injected electrons are trapped by oxygen/water molecules adsorbed on Ag/TiO_2 to yield the hydroxyl and superoxide radicals responsible for the photodegradation process. Because of their better photocatalytic and thermoelectric performance, this material is believed to be suitable replacement for Pani in a range of electrical and electronic devices.

ASSOCIATED CONTENT

Supporting Information

Structural refined data of TiO_2 in Ag/TiO_2@Pani, DC electrical conductivity of Pani and Ag/TiO_2@Pani, TEM, HR-TEM Ag/TiO_2, SEM of Pani and Ag/TiO_2@Pani, of DRS, XPS survey spectra, C 1s spectra, DTA, activation energy curve, and plot of C/C_0 versus the irradiation time for the photodegradation of MB. This material is available free of charge via the Internet at http://pubs.acs.org.

AUTHOR INFORMATION

Corresponding Author

*Tel:. +82-53-810-2517. Fax: +82-53-810-4631. E-mail: mhcho@ynu.ac.kr.

Notes

The authors declare no competing financial interest.

ACKNOWLEDGMENTS

This study was supported by Basic Science Research Program through the National Research Foundation of Korea (NRF) funded by the Ministry of Education, Science and Technology (Grant 2012R1A1A4A01005951).

REFERENCES

(1) Fujishima, A.; Honda, K. Electrochemical Photolysis of Water at a Semiconductor Electrode. *Nature* **1972**, *238*, 37−38.
(2) Kalathil, S.; Khan, M. M.; Ansari, S. A.; Lee, J.; Cho, M. H. Band Gap Narrowing of Titanium dioxide (TiO_2) Nanocrystals by Electrochemically Active Biofilms and their Visible Light Activity. *Nanoscale* **2013**, *5*, 6323−6326.
(3) Khan, M. M.; Ansari, S. A.; Amal, M. I.; Lee, J.; Cho, M. H. Highly Visible Light Active Ag@TiO_2 Nanocomposites Synthesized Using an Electrochemically Active Biofilm: A Novel Biogenic Approach. *Nanoscale* **2013**, *5*, 4427−4435.
(4) Ishiguro, H.; Nakano, R.; Yao, Y.; Kajioka, J.; Fujishima, A.; Sunada, K.; Minoshima, M.; Hashimoto, K.; Kubota, Y. Photocatalytic Inactivation of Bacteriophages by TiO_2-Coated Glass Plates under Low-Intensity, Long-Wavelength UV Irradiation. *J. Photochem. Photobiol. Sci.* **2011**, *10*, 1825−1829.
(5) Lee, M. S.; Hong, S. S.; Mohseni, M. Synthesis of Photocatalytic Nanosized TiO_2−Ag Particles with Sol−Gel Method using Reduction Agent. *J. Mol. Catal. A* **2005**, *242*, 135−140.
(6) Carneiro, J. O.; Teixeira, V.; Portinha, A.; Dupak, L.; Magalhaes, A.; Coutinho, P. Study of the Deposition Parameters and Fe-Dopant Effect in the Photocatalytic Activity of TiO_2 Films Prepared by DC Reactive Magnetron Sputtering. *Vacuum* **2005**, *78*, 37−46.
(7) Wu, JC-S.; Chen, C. H. A Visible-Light Response Vanadium-Doped Titania Nanocatalyst by Sol−Gel Method. *J. Photochem. Photobiol., A* **2004**, *163*, 509−515.
(8) Asahi, R.; Morikawa, T.; Ohwaki, T.; Aoki, K.; Taga, Y. Visible-Light Photocatalysis in Nitrogen-Doped Titanium Oxides. *Science* **2001**, *293*, 269−271.
(9) Wu, Z.; Dong, F.; Zhao, W.; Guo, S. Visible Light Induced Electron Transfer Process over Nitrogen Doped TiO_2 Nanocrystals Prepared by Oxidation of Titanium Nitride. *J. Haz. Mater.* **2008**, *157*, 57−63.
(10) Takeshita, K.; Yamakata, A.; Ishibashi, T.; Onishu, H.; Nishijima, K.; Ohno, T. Transient IR Absorption Study of Charge Carriers Photogenerated in Sulfur-Doped TiO_2. *J. Photochem. Photobiol.* **2006**, *177*, 269−275.
(11) Karácsonyi, É.; Baia, L.; Dombi, A.; Danciu, V.; Mogyorósi, K.; Pop, L. C.; Kovács, G.; Coşoveanu, V.; Vulpoi, A.; Simon, S.; Pap, Zs. The Photocatalytic Activity of TiO_2/WO_3/Noble Metal (Au or Pt) Nanoarchitectures Obtained by Selective Photodeposition. *Catal. Today* **2013**, *208*, 19−27.
(12) Rawal, S.B.; Bera, S.; Lee, W. I.; Jang, Du-J.; Lee, W. I. Design of Visible-Light Photocatalysts by Coupling of Narrow Bandgap Semiconductors and TiO_2: Effect of their Relative Energy Band Positions on the Photocatalytic Efficiency. *Catal. Sci. Technol.* **2013**, *3*, 1822−1830.
(13) Ronca, E.; Pastore, M.; Belpassi, L.; Tarantelli, F.; Angelis, F. D. Influence of the Dye Molecular Structure on the TiO_2 Conduction Band in Dye-Sensitized Solar Cells: Disentangling Charge Transfer and Electrostatic Effects. *Energy Environ. Sci.* **2013**, *6*, 183−193.
(14) Ali, O.; Sepideh, B.; Ali, E. Preparation, Characterization and Photocatalytic Activity of TiO_2/Polyaniline Core-Shell Nanocomposite. *Bull. Mater. Sci.* **2012**, *35*, 801−809.
(15) Peng, Wang.; Baibiao, Huang.; Ying, Dai.; Whangbo, M. H. Plasmonic Photocatalysts: Harvesting Visible Light with Noble Metal Nanoparticles. *Phys. Chem. Chem. Phys.* **2012**, *14*, 9813−9825.
(16) Tunc, I.; Bruns, M.; Gliemann, H.; Grunze, M.; Koelsch, P. Bandgap Determination and Charge Separation in Ag@TiO_2 Core Shell Nanoparticle Films. *Surf. Interface Anal.* **2010**, *42*, 835−841.
(17) Hari, M.; Joseph, S. A.; Mathew, S.; Radhakrishnan, P.; Nampoori, V. P. N. Band-Gap Tuning and Nonlinear Optical Characterization of Ag:TiO_2 Nanocomposites. *J. Appl. Phys.* **2012**, *212*, 74307−74314.
(18) Exarhos, G. J.; Rose, A.; Wang, L. Q.; Windisch, C. F., Jr Postdeposition Reduction of Noble Metal Doped ZnO Films. *J. Vac. Sci. Technol.* **1998**, *16*, 1926−1933.
(19) Kalathil, S.; Khan, M. M.; Lee, J.; Cho, M. H. Production of Bioelectricity, Bio-Hydrogen, High Value Chemicals and Bioinspired

Nanomaterials by Electrochemically Active Biofilm. *Biotechnol. Adv.* **2012**, *31*, 915−924.
(20) Khan, M. M.; Ansari, S. A.; Lee, J.; Cho, M. H. Novel Ag@TiO_2 Nanocomposite Synthesized by Electrochemically Active Biofilm for Nonenzymatic Hydrogen Peroxide Sensor. *Mater. Sci. Eng. C* **2013**, *33*, 4692−4699.
(21) Ansari, S. A.; Khan, M. M.; Kalathil, S.; Nisar, A.; Lee, J.; Cho, M. H. Oxygen Vacancy Induced Band Gap Narrowing of ZnO Nanostructures by an Electrochemically Active Biofilm. *Nanoscale* **2013**, *5*, 9238−9246.
(22) Robert, D.; Piscopo, A.; Heintz, O.; Weber, J. V. Photocatalytic Detoxification with TiO_2 Supported on Glass-Fibre by Using Artificial and Natural Light. *Catal. Today* **1999**, *54*, 291−296.
(23) Lee, C. S.; Kim, J.; Son, J.Y.; Choi, W.; Kim, H. Photocatalytic Functional Coatings of TiO_2 Thin Films on Polymer Substrate by Plasma Enhanced Atomic Layer Deposition. *Appl. Catal. B- Environ.* **2009**, *91*, 628−633.
(24) Ansari, M. O.; Khan, M. M.; Ansari, S. A.; Amal, I.; Lee, J.; Cho, M. H. *p*TSA Doped Conducting Graphene/Polyaniline Nanocomposite Fibers: Thermoelectric Behavior and Electrode Analysis. *Chem. Eng. J.* **2014**, *242*, 155−161.
(25) Xiong, P.; Chen, Q.; He, M.; Sun, X.; Wang, X. Cobalt Ferrite−Polyaniline Heteroarchitecture: a Magnetically Recyclable Photocatalyst with Highly Enhanced Performances. *J. Mater. Chem.* **2012**, *22*, 17485−17493.
(26) Ansari, M. O.; Mohammad, F. Thermal Stability of HCl-Doped-Polyaniline and TiO_2 Nanoparticles-Based Nanocomposites. *J. Appl. Polym. Sci.* **2012**, *124*, 4433−4442.
(27) Khan, M. M.; Ansari, S. A.; Lee, J. H.; Lee, J.; Cho, M. H. Mixed Culture Electrochemically Active Biofilms and their Microscopic and Spectroelectrochemical Studies. *ACS Sustainable Chem. Eng.* **2013**, *2* (3), 423−432.
(28) Pang, S.; Li, G.; Zhang, Z. Synthesis of Polyaniline-Vanadium Oxide Nanocomposite Nanosheets. *Macromol. Rapid Commun.* **2005**, *26*, 1262−1265.
(29) Ansari, M. O.; Yadav, S. K.; Cho, J. W.; Mohammad, F. Thermal Stability in Terms of DC Electrical Conductivity Retention and the Efficacy of Mixing Technique in the Preparation of Nanocomposites of Graphene/Polyaniline over the Carbon Nanotubes/Polyaniline. *Compos. Part B-Eng.* **2013**, *47*, 155−161.
(30) Liu, J.; Gao, Y.; Cao, D.; Zhang, L.; Guo, Z. Nanoparticle Dispersion and Aggregation in Polymer Nanocomposites: Insights from Molecular Dynamics Simulation. *Langmuir* **2011**, *27*, 7926−7933.
(31) Gupta, K.; Jana, P. C.; Meikap, A. K. Optical and Electrical Transport Properties of Polyaniline−Silver Nanocomposite. *Synthetic Met.* **2010**, *160*, 1566−1573.
(32) Sun, Y. Controlled Synthesis of Colloidal Silver Nanoparticles in Organic Solutions: Empirical Rules for Nucleation Engineering. *Chem. Soc. Rev.* **2013**, *42*, 2497−2511.
(33) Wong, H. C.; Cabral, J. T. Spinodal Clustering in Thin Films of Nanoparticle-Polymer Mixtures. *Phys. Rev. Lett.* **2010**, *105*, 38301−38304.
(34) Cantor, B.; Doherty, R. D. Heterogeneous Nucleation in Solidifying Alloys. *Acta Metall.* **1979**, *27*, 33−46.
(35) Turnbull, D. Formation of Crystal Nuclei in Liquid Metals. *J. Appl. Phys.* **1950**, *21*, 1022−1028.
(36) Ansari, M. O.; Khan, M. M.; Ansari, S. A.; Amal, I.; Lee, J.; Cho, M. H. Enhanced Thermoelectric Performance and Ammonia Sensing Properties of Sulfonated Polyaniline/Graphene Thin Films. *Mater. Lett.* **2014**, *114*, 159−162.
(37) Spurr, R. A.; Myers, H. Quantitative Analysis of Anatase-Rutile Mixtures with an X-Ray Diffractometer. *Anal. Chem.* **1957**, *29*, 760−762.
(38) Carvajal, R. Recent Advances in Magnetic Structure Determination by Neutron Powder Diffraction. *Phys. B* **1993**, *192*, 55−69.
(39) Cullity, B. D.; Stock, S. R. *Elements of X-ray Diffraction*, 3rd ed.; Prentice Hall: NJ, 2001; Chapter 4, pp 123−157.
(40) Mallick, K.; Witcomb, M.; Scurrell, M. Palladium-Polyaniline and Palladium-Polyaniline Derivative Composite Materials. *Platinum Metals Rev.* **2007**, *51*, 3−15.
(41) Chuang, F. Y.; Yang, S. M. Titanium Oxide and Polyaniline Core-Shell Nanocomposites. *Synth. Met.* **2005**, *152*, 361−364.
(42) Macdiarmid, A.G.; Chiang, J.C.; Richter, A.F.; Epstein, A. J. Polyaniline: a New Concept in Conducting Polymers. *Synth. Met.* **1987**, *18*, 285−290.
(43) Ansari, M. O.; Mohammad, F. Thermal Stability, Electrical Conductivity and Ammonia Sensing Studies on *p*-Toluenesulfonic Acid Doped Polyaniline:Titanium dioxide (*p*TSA/Pani:TiO_2) Nanocomposites. *Sens. Actuators, B* **2011**, *157*, 122−129.
(44) Scocioreanu, M.; Baibarac, M.; Baltog, I.; Pasuk, I.; Velula, T. Photoluminescence and Raman Evidence for Mechanico-Chemical Interaction of Polyaniline-Emeraldine Base with ZnS in Cubic and Hexagonal Phase. *J. Solid State Chem.* **2012**, *186*, 217−223.
(45) Liqiang, J.; Yichun, Q.; Baiqi, W.; Shudan, L.; Baojiang, J.; Libin, Y.; Wei, F.; Honggang, F.; Jiazhong, S. Review of Photoluminescence Performance of Nano-Sized Semiconductor Materials and its Relationships with Photocatalytic Activity. *Sol. Energy Mater. Sol. Cells* **2006**, *90*, 1773−1787.
(46) Kumar, R. V.; Mastai, Y.; Diamant, Y.; Gedanken, A. Sonochemical Synthesis of Amorphous Cu and Nanocrystalline Cu_2O Embedded in a Polyaniline Matrix. *J. Mater. Chem.* **2001**, *11*, 1209−1213.
(47) Rangraj, A.; Vangani, V.; Rakshit, K. Synthesis and Characterization of some Water Soluble Polymers. *J. Appl. Polym. Sci.* **1997**, *1*, 45−56.
(48) Abthagir, P.S.; Saraswathi, R.; Sivakolunthu, S. Aging and Thermal Degradation of Poly(*N*-Methylaniline). *Therm. Chim. Acta* **2004**, *2*, 109−123.
(49) Wanga, D.; Xiaoa, L.; Luoa, Q.; Lia, X.; Ana, J.; Duanb, Y. Highly Efficient Visible Light TiO_2 Photocatalyst Prepared by Sol−Gel Method at Temperatures Lower than 300 °C. *J. Hazard. Mater.* **2011**, *192*, 150−159.
(50) Nagaraja, M.; Pattar, J.; Shashank, N.; Manjanna, J.; Kamada, Y.; Rajanna, K.; Mahesh, H. M. Electrical, Structural and Magnetic Properties of Polyaniline/pTSA-TiO_2 Nanocomposites. *Synth. Met.* **2009**, *159*, 718−722.
(51) Bai, X.; Wang, L.; Zong, R.; Lv, Y.; Sun, Y.; Zhu, Y. Performance Enhancement of ZnO Photocatalyst via Synergic Effect of Surface Oxygen Defect and Graphene Hybridization. *Langmuir* **2013**, *29*, 3097−3105.
(52) Khan, M. M.; Ansari, S. A.; Pradhan, D.; Omaish, M.; Han, D. H.; Lee, J.; Cho, M. H. Band Gap Engineered TiO_2 Nanoparticles for Visible Light Induced Photoelectrochemical and Photocatalytic Studies. *J. Mater. Chem. A* **2014**, *2*, 637−644.
(53) Gan, J.; Lu, X.; Wu, J.; Xie, S.; Zhai, T.; Yu, M.; Zhang, Z.; Mao, Y.; Wang, S. C.; Shen, Y.; Tong, Y. Oxygen Vacancies Promoting Photoelectrochemical Performance of In_2O_3 Nanocubes. *Sci. Rep.* **2013**, *3*, 1021−1028.
(54) Khan, Z.; Chetia, T. R.; Qureshi, M. Rational Design of Hyperbranched 3D Heteroarrays of SrS/CdS: Synthesis, Characterization and Evaluation of Photocatalytic Properties for Efficient Hydrogen Generation and Organic Dye Degradation. *Nanoscale* **2012**, *4*, 3543−3550.
(55) Zhang, H.; Zong, R.L.; Zhao, J. A.; Zhu, Y.F. Dramatic Visible Photocatalytic Degradation Performances due to Synergetic Effect of TiO_2 with PANI. *Environ. Sci. Technol.* **2008**, *42*, 3803−3807.
(56) Ansari, S. A.; Khan, M. M.; Lee, J.; Cho, M. H. *J. Ind. Eng. Chem.* **2014**, *20*, 1602−1607.
(57) Yang, Y.; Wen, J.; Wei, J.; Xiong, R.; Shi, J.; Pan, C. Polypyrrole-Decorated Ag-TiO_2 Nanofibers Exhibiting Enhanced Photocatalytic Activity under Visible-Light Illumination. *ACS Appl. Mater. Interfaces* **2013**, *5*, 6201−6207.
(58) Ansari, S. A.; Khan, M. M.; Ansari, M. O.; Lee, J.; Cho, M. H. Biogenic Synthesis, Photocatalytic, and Photoelectrochemical Performance of Ag−ZnO Nanocomposite. *J. Phys. Chem. C* **2013**, *117*, 27023−27030.

(59) Ansari, S. A.; Khan, M. M.; Ansari, M. O.; Lee, J.; Cho, M. H. Highly Photoactive SnO_2 Nanostructures Engineered by Electrochemically Active Biofilm. *New J. Chem.* **2014**, *38*, 2462−2469.
(60) Ansari, S. A.; Khan, M. M.; Ansari, M. O.; Kalathil, S.; Lee, J.; Cho, M. H. Band Gap Engineering of CeO_2 Nanostructure Using an Electrochemically Active Biofilm for Visible Light Applications. *RSC Adv.* **2014**, *4*, 16782−16791.
(61) Khan, M. M.; Ansari, S. A.; Omaish Min, B. K.; Lee, J.; Cho, M. H. Biogenic Fabrication of Au@CeO_2 Nanocomposite with Enhanced Visible Light Activity. *J. Phys. Chem. C* **2014**, *118*, 9477−9484.